Journal for ImmunoTherapy of Cancer

PDZ domains of PATJ facilitate immunological synapse formation to promote T cell activation

Xinxin Xiong [1,2] Danyang Wang,[1] Liping Xu,[1] Siyu Chen,[3] Jingjing He,[2] Xiaomin Zhang,[1] Ziqian Fang,[1] Jianeng Zhang,[1] Wende Li,[1] Penghui Zhou[1]

To cite: Xiong X, Wang D, Xu L, *et al*. PDZ domains of PATJ facilitate immunological synapse formation to promote T cell activation. *Journal for ImmunoTherapy of Cancer* 2025;**13**:e010966. doi:10.1136/jitc-2024-010966

► Additional supplemental material is published online only. To view, please visit the journal online (https://doi.org/10.1136/jitc-2024-010966).

XX and DW contributed equally.

Accepted 16 April 2025

[1]Sun Yat-sen University Cancer Center, Guangzhou, Guangdong, China
[2]Medical Research Institute, Guangdong Provincial People's Hospital (Guangdong Academy of Medical Sciences), Southern Medical University, Guangzhou, Guangdong, China
[3]Guangdong Laboratory Animals Monitoring Institute, Guangzhou, Guangdong, China

Correspondence to
Professor Penghui Zhou; zhouph@sysucc.org.cn

Wende Li; lwd@gdlami.com

ABSTRACT

Background The highly organized structures of the immunological synapse (IS) are crucial for T cell activation. PDZ domains might be involved in the formation of the IS by serving as docking sites for protein interactions. In this study, we investigate the role of the PALS1-associated tight junction protein (PATJ), which contains 10 PDZ domains, in the formation of IS and its subsequent impact on T cell activation.

Methods To elucidate the function of PATJ, we generated murine models with conditional T cell-specific knockout of *Patj* and assessed T cell activation both *in vitro* and *in vivo* within the context of infection and cancer. We employed confocal microscopy to visualize the formation of IS between T cells and antigen-presenting cells in the absence of *Patj*. A series of PATJ truncations containing different combinations of PDZ domains was used to identify the minimal domain required for effective T cell receptor signaling. The identified active PDZ domain was then incorporated into mesothelin (MSLN)-specific chimeric antigen receptor (CAR) to evaluate its impact on CAR-T cell cytotoxicity against solid tumors.

Results We observed a rapid increase in PATJ expression during T cell activation. Conditional knockout of *Patj* in T cells showed impaired immunity against infection and cancer in murine models. Mechanistically, ablation of *Patj* impedes IS formation, and thus reduces T cell activation. We further showed that engineering the active PDZ domain of PATJ into CAR structure significantly promoted the effector function of CAR-T cells.

Conclusions Our study reveals an important role of PATJ in the formation of IS and provides an approach to improve the efficacy of CAR-T therapy.

WHAT IS ALREADY KNOWN ON THIS TOPIC

⇒ T cell activation is initiated with the formation of immunological synapse (IS). PDZ domains might be involved in the formation of IS by protein interactions. However, the specific role of PALS1-associated tight junction protein (PATJ), which contains 10 PDZ domains, in the formation of IS and its subsequent impact on T cell activation was not well understood.

WHAT THIS STUDY ADDS

⇒ This study demonstrates that *Patj*-deficient T cells exhibit impaired immunity against infections and cancer in murine models. Mechanistic investigations reveal that conditional knockout of *Patj* in T cells impairs the formation of IS, thereby attenuating T cell activation. Furthermore, this study identifies the minimal active PDZ domain of PATJ that is essential for effective T cell receptor signaling. Engineering this PDZ domain into the chimeric antigen receptor (CAR) structure significantly enhances the effector functions of CAR-T cells against solid tumors.

HOW THIS STUDY MIGHT AFFECT RESEARCH, PRACTICE OR POLICY

⇒ The findings not only provide novel insights into the role of PATJ in IS formation and T cell activation, but also offer a potential strategy to enhance the efficacy of CAR-T therapy against solid tumors.

INTRODUCTION

Immune synapse (IS) formation is essential for initiating T cell immunity, which plays an important role in antitumor immune responses.[1] Different synapse structures formed during antigen recognition might trigger variable downstream signaling, and thus lead to distinct function and fates of T cells after activation.[2]

The PDZ domain, a conserved structural motif in diverse organisms,[3] is named using the initials of three proteins—postsynaptic density 95 (PSD-95), discs large (Dlg), and zonula occludens-1 (ZO-1). It consists of 80–100 amino acids forming two alpha helices and six beta strands.[4] This domain mediates protein clustering and interactions on cellular membranes. It is categorized into three groups: proteins with only PDZ domains, those with additional domains like SH3 and Guk (which lacks catalytic activity but aids protein interactions), and those with other domains such as L27, PH, and C2.[5] PDZ-rich proteins are crucial for regulating complex protein interactions, essential for signal transduction, cell division, junction formation, and cytoskeletal organization.[6]

PDZ domain-containing proteins like Scrib and Dlg1 are rapidly recruited to the IS on

T cell activation.[7–9] Crtam also plays a role in synapse formation by interacting with Scrib's third PDZ domain through its C-terminal ESIV motif, thus regulating T cell activation and function.[10] Additionally, PDZ binding motifs in chimeric antigen receptors (CARs) can optimize the synapse for effective solid tumor CAR T therapy.[11] PALS1-associated tight junction (PATJ, a protein with 10 PDZ domains and one L27 domain, acts as a platform for protein interactions.[12] In epithelial cells, it localizes near the membrane to form a complex with PAR-3/PAR-6/Cdc42/aPKC/PALS1, maintaining cellular polarity by preventing membrane component exchange.[13] However, the function of PATJ in immune cells, particularly T cells, remains unexplored.

We observed a rapid increase in PATJ expression on T cell activation, suggesting a potent role of PATJ in T cell immunity. Indeed, *Patj*-deficient OT-I T cells showed decreased proliferation and reduced function during *Listeria monocytogenes* expressing ovalbumin (LM-OVA) infection. Mice with conditional knockout of *Patj* in T cells also showed impaired antitumor T cell immunity and increased tumor growth. Prolonged IS formation and reduced cytokine secretion were observed in *Patj*-deficient T cells. Our data indicate that *Patj* might enhance T cell function via the PDZ domain-mediated interactions of synapse proteins. Therefore, we engineered the active PDZ domain into the CAR structure, and found this PDZ domain of PATJ significantly increased the effector function of CAR-T cells. Our study highlights PATJ's critical role in infection and cancer immunity by facilitating IS formation.

METHODS AND MATERIALS

Cell lines

The B16 murine melanoma cell line, MC38 colon carcinoma cell line, human lung cancer cell line A549, and HEK293T cells were acquired from the American Type Culture Collection (Manassas, Virginia, USA). The B16-OVA cells were produced by transducing B16 cells with a lentiviral vector encoding OVA protein, followed by selection using puromycin. The $A549^{MSLN\text{-}GFP\text{-}luciferase}$ cells were generated by transducing A549 cells with a lentiviral vector encoding mesothelin (MSLN), green fluorescent protein (GFP), and luciferase which were selected using puromycin. These cells were routinely cultured in Dulbecco's Modified Eagle Medium (DMEM, Gibco, USA) or Roswell Park Memorial Institute 1640 Medium (RPMI-1640, Gibco, USA), both supplemented with 10% fetal bovine serum (FBS, Gibco, USA), 1% penicillin-streptomycin, 2 mM L-glutamine, and 1 mM sodium pyruvate (Gibco, USA). The cultures were maintained at 37°C in an atmosphere of 5% CO_2. Mycoplasma contamination was confirmed to be absent in all the cell lines.

Mice

The C57BL/6J and NSG mice (female, age 4–6 weeks, 18–20 g) were obtained from Charles River Laboratory (Beijing, China). The $CD4^{Cre}$ and OT-I (CD45.1+) transgenic mouse strains were acquired from the Jackson Laboratory (Bar Harbor, Maine, USA). To create mice with a conditional knockout of *Patj* in T cells, *Patj* floxed mice were bred with $CD4^{Cre}$ mice. The $Patj^{CKO}$ OT-I mice were produced by crossing $Patj^{CKO}$ mice with CD45.1+ OT-I mice. All mice were kept in a specific pathogen-free facility at Sun Yat-sen University (Guangzhou, China). The animal experimentation protocols were reviewed and approved by the Institutional Animal Care and Use Committee at Guangdong Provincial People's Hospital (KY-Z-2022-215-01) to ensure compliance with ethical guidelines for animal research.

T cell activation

The peripheral blood mononuclear cells (PBMCs) were cultured in complete RPMI 1640 medium supplemented with interleukin-2 (IL-2) (200 IU/mL, PeproTech, USA) and consisting of RPMI 1640, 10% FBS, 20 mM HEPES, 1 mM sodium pyruvate, 0.05 mM 2-mercaptoethanol, 2 mM L-glutamine, and 100 µg/mL each of streptomycin and penicillin. Cells were then seeded in 96-well plates coated with human CD3/28 antibodies (5 µg/mL, Novoprotein, Suzhou, China) for activation. Mouse CD8+T cells were isolated from the splenocytes and lymphocytes using magnetic bead purification with a mouse CD8+ T cell isolation kit (BioLegend, San Diego, California, USA), following the manufacturer's protocol. The purified CD8+T cells were activated *in vitro* for 48 hours with immobilized anti-CD3/CD28 antibodies (5 µg/mL, Invitrogen, USA) in complete RPMI 1640 medium. On day 2, carboxyfluorescein succinimidyl ester (CFSE, Thermo Fisher, USA) dilution assay and intracellular staining were performed to assess T cell proliferation and activation status.

In vivo mouse experiments

C57BL/6J mice (n=6/per group) were subcutaneously (s.c.) injected with 2×10^5 B16, B16-OVA, or MC38 tumor cells resuspended in 200 µL phosphate-buffered saline (PBS). The volume of the tumors was measured every 2 days using the modified ellipsoidal formula: (Length×Width × Width)/2. Mice with a tumor longest axis exceeding 20 mm were euthanized to adhere to ethical standards.

For the adoptive transfer of OT-I T cells, 1×10^6 cells were administered intravenously to mice with B16-OVA melanoma. In pathogen-induced infections, 5×10^3 plaque-forming units of LM-OVA were injected intravenously, followed by the intravenous transfer of 5×10^4 OT-I T cells 24 hours later.

Tumor digestion and single-cell suspensions preparation

Tumor samples were carefully cut into small pieces using sterile surgical blades. The minced tumors were then treated with a specially formulated dissociation buffer containing 50 U/mL of Collagenase Type IV (Invitrogen, California, USA) and 20 U/mL of DNase (Roche,

Indianapolis, Indiana, USA). This mixture was incubated at 37°C for 1 hour with gentle agitation to facilitate the breakdown process. After incubation, the samples were further processed using the gentleMACS dissociator (Miltenyi Biotech, Bergisch Gladbach, Germany) to separate cells completely. The resulting cell suspensions were filtered through a 70 µm strainer to remove undigested tissue or aggregates. Postfiltration, the cells were washed three times with PBS to remove residual enzymes or debris. The cleaned cell suspensions were finally separated using Percoll (Sigma-Aldrich, USA) in a density-gradient centrifugation to isolate the viable cells.

Flow cytometry

To detect the surface markers, cells were incubated with the indicated antibodies for 30 min at 4°C and subsequently analyzed using a LSRFortessa X-20 flow cytometer (BD Biosciences; Franklin Lakes, New Jersey, USA). Cells were first fixed and permeabilized for intracellular staining using the BD Cytofix/Cytoperm Fixation/Permeabilization Kit according to the manufacturer's instructions. Then, incubate with antibodies and analyze the samples. All antibodies used in these assays were purchased from BioLegend (BioLegend; San Diego, California, USA).

RNA isolation and real-time quantitative PCR

Total RNA was extracted from T cells using the TRIZOL reagent (Invitrogen, California, USA) following the manufacturer's protocols. The concentration and purity of the RNA were assessed using a Nanodrop spectrophotometer. Subsequently, reverse transcription was performed using the complementary DNA (cDNA) Synthesis Kit (Vazyme, Nanjing, China). Quantitative real-time PCR analysis was carried out using the SYBR green master mix (TransGen Biotech, Beijing, China) on a Bio-Rad instrument. The expression levels of targeted genes were normalized against β-actin as an internal control. The following primers are used:

Mouse Patj forward primer: 5'-GGAAGATTTGCC TCTGTACCGAC-3'

Mouse Patj reverse primer: 5'-GCTGAAGTTCGGTGTC TCCTCT-3'

Mouse CD2 forward primer: 5'-GATGAGAAACGA CAGTGGCACC-3'

Mouse CD2 reverse primer: 5'-CCAGTGGATCAT GGGCTTTGAG-3'

Mouse CD28 forward primer: 5'-CGCCTTACCTAG ACAACGAGAG-3'

Mouse CD28 reverse primer: 5'-AAACAGGACTCC AGCAACCACG-3'

Mouse CD45 forward primer: 5'-CTTCAGTGGTCC CATTGTGGTG-3'

Mouse CD45 reverse primer: 5'-TCAGACACCTCT GTCGCCTTAG-3'

Mouse ICOS forward primer: 5'-GCAGCTTTCGTT GTGGTACTCC-3'

Mouse ICOS reverse primer: 5'-TGTGTTGACTGC CGCCATGAAC-3'

β-actin forward primer: 5'-CATTGCTGACAGGATG CAGAAGG-3'

β-actin reverse primer: 5'- TGCTGGAAGGTGGACA GTGAGG-3'

Western blotting

Cells were lysed in ice-cold RIPA lysis buffer (Invitrogen, USA) supplemented with protease inhibitors and a phosphatase inhibitor cocktail (Roche). The extracted proteins were separated using 10% SDS–polyacrylamide gel electrophoresis and subsequently transferred to polyvinylidene difluoride membranes (Millipore, USA). The membranes were blocked with 5% bovine serum albumin (BSA, Sigma, USA). Subsequently, the membranes were incubated overnight with primary antibodies (all purchased from Cell Signaling Technology, USA). The following day, the membranes were washed three times with TBST buffer (10 mM Tris-HCl, pH 8.0, 150 mM NaCl, 0.1% (v/v) Tween-20) and then incubated with horseradish peroxidase-conjugated secondary antibodies (Cell Signaling Technology, USA) for 1 hour. The signals were detected using the enhanced chemiluminescence substrate (Millipore) and captured using a ChemiDoc imaging system (Bio-Rad).

Plasmids and DNA constructs

To construct the truncated mutants of the mouse PATJ PDZ domain, the PDZ1 and PDZ2 sequence (TC1) was subcloned into the pMIG-EFs-Flag-hPGK-mThy1.1 retroviral vector using the following primers: Forward primer: 5'-GCCACCATGCCTGAAAACCCTGCT-3'; Reverse primer: 5'-TCAAGGGTCTCTGGCCAC-3'. Similarly, the PDZ3 and PDZ4 sequence (TC2) was subcloned using these primers: Forward primer: 5'-GCCACCAT GGTTGGTGAAATTGCAGTAACAC-3'; Reverse primer: 5'-TCACAGCCGGCGGCA-3'. The PDZ5 sequence (TC3) was subcloned using these primers: Forward primer: 5'-GCCACCATGTTTGATGATGAGGCCTCAGTTGATG-3'; Reverse primer: 5'-TCAATTCTTGGTGGACCCCAG-3'. Additionally, the PDZ6 and PDZ7 sequence (TC4) was subcloned using these primers: Forward primer: 5'-GCCA CCATGAGTTGAAATTTTTAGAGAACCTAATGTG; Reverse primer: 5'-TCAATCATTTCCTGGCCAGGGA-3'. Lastly, the PDZ8 to PDZ10 sequence (TC5) was subcloned using these primers: Forward primer: 5'- GCCACCAT GCATAGAAATATCCAAGGGACGC-3'; Reverse primer: 5'-TCAATCAGCCGTCCTCTGCA-3'. The integrity of all constructs was verified by sequencing (RuiBiotech, Beijing, China).

Retroviral transduction of mouse CD8+ T cells

To produce retrovirus, HEK293-T cells were cultured in 10 cm dishes using complete DMEM media. The pMIG-EFs-hPGK-mThy1.1 expression plasmid (Addgene, USA) or the recombined pMIG-EFs-PATJ truncate-hPGK-mThy1.1 expression plasmid was co-transfected with the

pCL-Eco packaging plasmid (Addgene) using PEI reagent. Supernatants containing retrovirus were collected at 48 and 72 hours post-transfection to infect activated CD8+T cells. Mouse CD8+ T lymphocytes were isolated using the Mouse CD8+ T cell isolation kit (BioLegend) and cultured in complete RPMI 1640 media. The purified cells were activated with plate-bound CD3/28 antibodies (5 µg/mL) for 24 hours. Then, they underwent spin culture with the retroviral supernatant in the presence of plate-coated RetroNectin (Takara, Japan) and polybrene (4 µg/mL, Yeasen, China). The transduced cells were expanded in complete RPMI 1640 media for subsequent experiments.

To overexpress LFA-1 in *Patj*^{CKO} OT-I T cells, the pMIG-EFs-LFA-1^{OE}-hPGK-mThy1.1 expression plasmid was co-transfected with the pCL-Eco packaging plasmid into 293 T cells using PEI. Retroviral supernatants were subsequently collected and used to infect preactivated *Patj*^{CKO} OT-I T cells, following the established protocol. The transduced T cells were then expanded in complete RPMI 1640 medium and positive cells were sorted for using mThy1.1 antibody via a BD FACSAria II in subsequent experiments.

Immunofluorescent staining

For immunofluorescence labeling, cells were fixed with 4% PFA (Beyotime, China) at room temperature for 15 min and washed with PBS three times. Then, the cells were permeabilized with 0.1% Triton X-100 for 15 min and blocked with 3% BSA (Sigma, USA) for 30 min at room temperature. Cells were incubated with primary antibodies at 4°C overnight and then with the corresponding fluorophore-conjugated secondary antibodies for 60 min. Imaging of the cells was performed using a Carl Zeiss Laser Scanning Microscope 710 (Oberkochen, Germany). Image processing and quantifying the immunofluorescence signals were conducted using ZEN 2.3 SP1 software (Carl Zeiss, Germany).

Primary T cells-B cells conjugated formation

B and T cells obtained from the spleens and lymph nodes of wild-type (WT) OT-I mice and *Patj*^{CKO} OT-I mice were sorted using a BD FACSAria II. Subsequently, the cells were incubated with 1 µg/mL of $OVA_{257–264}$ (SIINFEKL) peptides (GenScript, Nanjing, China) at 37°C and maintained a cell ratio of 1:1. The cells were then stained with CD3-FITC, CD19-PE, and LFA-1-APC for 30 min at 4°C in the dark. After three washes with PBS, the cells were imaged using a Carl Zeiss Laser Scanning Microscope 710 equipped with a×63 oil immersion objective. Image processing and quantification of the immunofluorescence signals were performed using ZEN V.2.3 SP1 software.

Cytotoxicity assay

Cytotoxicity was evaluated by quantifying the lactate dehydrogenase released into the cell culture medium using the CytoTox 96 Non-Radioactive Cytotoxicity Assay kit (Promega, Wisconsin, USA), following the manufacturer's instructions. 1000 A549 target cells were co-cultured with effector T cells at various effector-to-target (E:T) ratios for 24 hours in a 96-well plate. Subsequently, 50 µL of supernatant from each well was mixed with 50 µL of the CytoTox 96 reagent and incubated for 30 min at room temperature in the dark. Afterward, 50 µL of stop solution was added to each well. The percentage of specific lysis was calculated using the following formula: %Cytotoxicity = (Experimental – Effector Spontaneous – Target Spontaneous) / (Target Maximum – Target Spontaneous) × 100.

Construction of PATJ truncate mesothelin-specific CAR-T cells

To engineer the PATJ truncate MSLN-targeting CAR constructs (hMSLN scFV-hCD28-hCD3-2A-PATJ TC1-hPGK-mThy1.1), the DNA sequence encoding the truncated domain of human PATJ (Forward primer: 5'-GCCA CCATGTATAGATATAGAACGGC-3'; Reverse primer: 5'-TCATGGATCTCTAGCAACGAG') was inserted into the lentiviral expression vector pHAGE-hMSLN scFV-hCD28-hCD3-hPGK-mThy1.1. Viral particles were produced by transfecting HEK 293 T cells with the pSPAX2 (Addgene) and pMD2.G (Addgene) packaging plasmids at a 5/3/2 ratio and the CAR expression plasmid using PEI as a transfection reagent. Six hours post-transfection, the cells were maintained in fresh complete DMEM. The cell culture supernatants containing the viral particles were harvested at 24 and 48 hours, pooled, filtered through a 45 µm filter using a vacuum system, and then centrifuged at 10,000 g for 90 min. Purified CD8+ T cells were subjected to spin infection with the lentivirus encoding the PATJ truncate MSLN-specific CAR in 24-well plates coated with retronectin and polybrene. Following infection, the genetically modified CAR-T cells were cultivated in a complete RPMI 1640 medium supplemented with IL-2. The surface expression of the PATJ truncate MSLN-specific CAR was confirmed by detecting the Thy1.1 (mouse CD90.1) marker using flow cytometry. Subsequently, the cells were cryopreserved for future use in designated experimental settings.

Repeated challenge assay of CAR-T cells

PBMCs were infected with either MSLN-CAR or PATJ TC1 MSLN-CAR lentivirus and maintained in T-cell medium for at least 10 days prior to the experiment. 4 hours after seeding the A549$^{MSLN\text{-}GFP\text{-}luciferase}$ cells (500,000 cells per 12 well plate), CAR-T cells were added at an E:T ratio of 2:1. Blank groups received an equivalent number of non-infected T cells. Every 48 hours, the T cells were removed, counted, and reincubated with A549$^{MSLN\text{-}GFP\text{-}luciferase}$ cells at the same 2:1 E:T ratio. This process was repeated for a total of five rounds of stimulation. After each round of stimulation, the remaining target cells were lysed using the Luciferase Cell Culture Lysis Reagent and stored at −80°C. Cytotoxicity was subsequently analyzed using the Luciferase Assay System (Promega) according to the manufacturer's instructions. The percentage of cytotoxicity

was calculated using the following formula: %Cytolysis = (Luciferase$_{Blank}$−Luciferase$_{CAR\text{-}T}$/(Luciferase$_{Blank}$)×100.

CAR-T cell synapse formation

T cells were transduced with MSLN-CAR or PATJ-TC1-MSLN-CAR lentivirus. Positively sorted cells were subsequently sorted using a BD FACSAria II. Meanwhile, A549$^{MSLN\text{-}EGFP}$ target cells were seeded into 35 mm confocal dishes (Corning, USA). The CAR-T cells were prestained with CD3-PE and LFA-1-APC antibodies and then co-cultured with target cells at a 1:1 ratio for an additional 30 min. The co-culture was imaged using a Carl Zeiss Laser Scanning Microscope 710 equipped with a ×63 oil immersion objective. Image processing and quantification of immunofluorescence signals were performed using ZEN V.2.3 SP1 software.

Statistical analysis

Data were analyzed using GraphPad Prism software (V.8; GraphPad Software, San Diego, California, USA). Statistical significance was set at p<0.05. Two groups were compared using an unpaired, two-tailed Student's t-test. For comparisons involving three or more groups, analyses were performed using one-way analysis of variance (ANOVA) or two-way ANOVA.

RESULTS

PATJ is highly expressed in CD8+ effector T cells

We initially investigated the expression of PATJ across various immune cell subsets within human blood and bone marrow, using existing RNA-sequencing datasets sourced from the Cancer Genome Atlas database. We found that PATJ is mainly expressed in CD8+ and CD4+ T cells (figure 1A). Interestingly, the highest levels of PATJ were observed in the CD8+ effector subset, while both naïve and memory CD8+ T cells expressed lower levels of PATJ (figure 2B). Subsequently, we isolated various immune cell subtypes, including dendritic cells, monocytes, B cells, CD8+ T cells, CD4+ T cells, and natural killer (NK) cells from WT C57BL/6J mice and measured their Patj levels using quantitative PCR (qPCR). Consistent with human data, the high level of Patj was detected in mouse CD8+ T cells (figure 1C). These results suggest that PATJ plays a crucial role in the effector function of CD8+ T cells.

To further elucidate the role of Patj in CD8+ T cells, we examined its expression over time *in vitro* following activation with anti-CD3/28 antibodies. The PATJ protein is upregulated in 12 hours after anti-CD3/CD28 activation (figure 1D, right), while the increase of Patj messenger RNA (mRNA) level is detected at 6 hours (figure 1D, left). This expression pattern suggested that Patj is involved in the early activation of CD8+ T cells. In addition, we found that CD8+ T cells lacking *Patj* (*Patj*^{CKO}) showed impaired

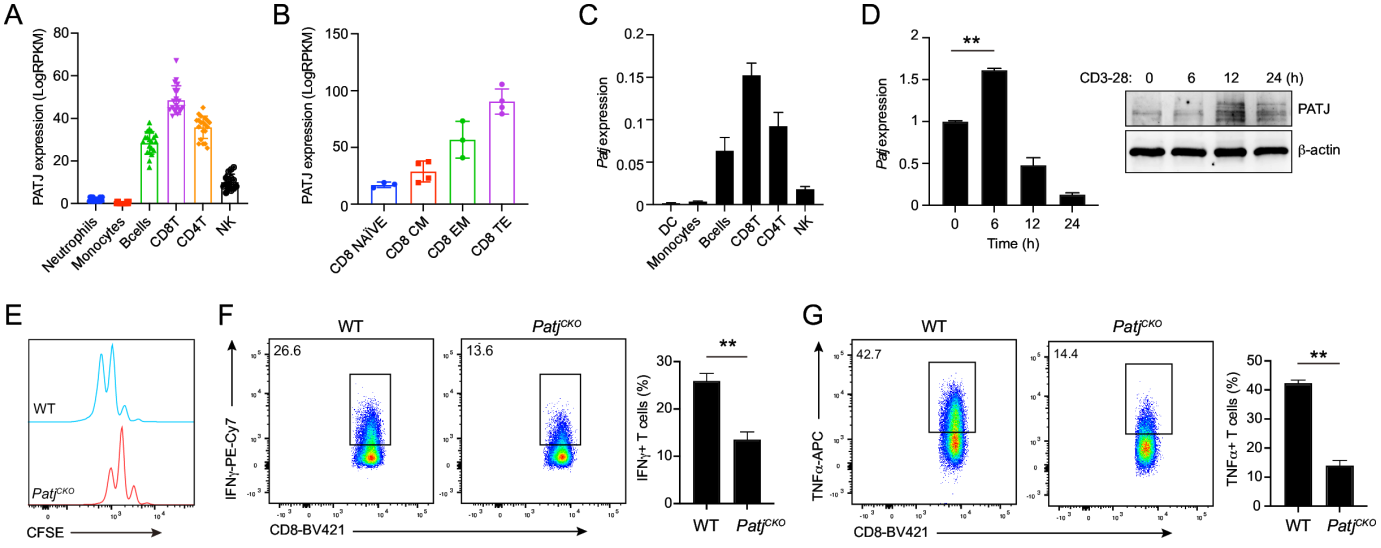

Figure 1 PATJ is highly expressed in CD8+ effector T cells. (A–B) Bulk RNA sequencing data indicating PATJ expression in sorted cell populations from human donor whole blood (A; GSE60424) and PBMCs (B; GSE107011). (C) qPCR analysis of Patj expression in sorted cell populations from various tumor-infiltrating immune subsets in a mouse melanoma model. (D) Patj mRNA (left) and protein (right) expression levels in CD8+ T cells isolated from the spleen and lymph nodes of C57BL/6J mice, assessed prior to activation and at specified time points following stimulation with anti-CD3/CD28 antibodies. (E) Proliferation rates of CD8+ T cells derived from the spleen and lymph node of WT or *Patj*^{CKO} mice after 24 hours of activation with anti-CD3/CD28 antibodies. (F–G) Intracellular protein expression profiles of CD8+ T cells from the spleen and lymph nodes of WT or *Patj*^{CKO} mice following 24 hours of activation with anti-CD3/CD28 antibodies. Data are presented as mean±SD. Statistical significance was determined using one-way ANOVA and unpaired Student's t-tests. **p<0.01. ANOVA, analysis of variance; CFSE, carboxyfluorescein succinimidyl ester; CM, central memory; DC, dendritic cell; EM, effector memory; IFNγ, interferon-gamma; mRNA, messenger RNA; NK, natural killer; PATJ, PALS1-associated tight junction protein; PBMC, peripheral blood mononuclear cell; qPCR, quantitative PCR; TE, terminal effector cells; WT, wild type.

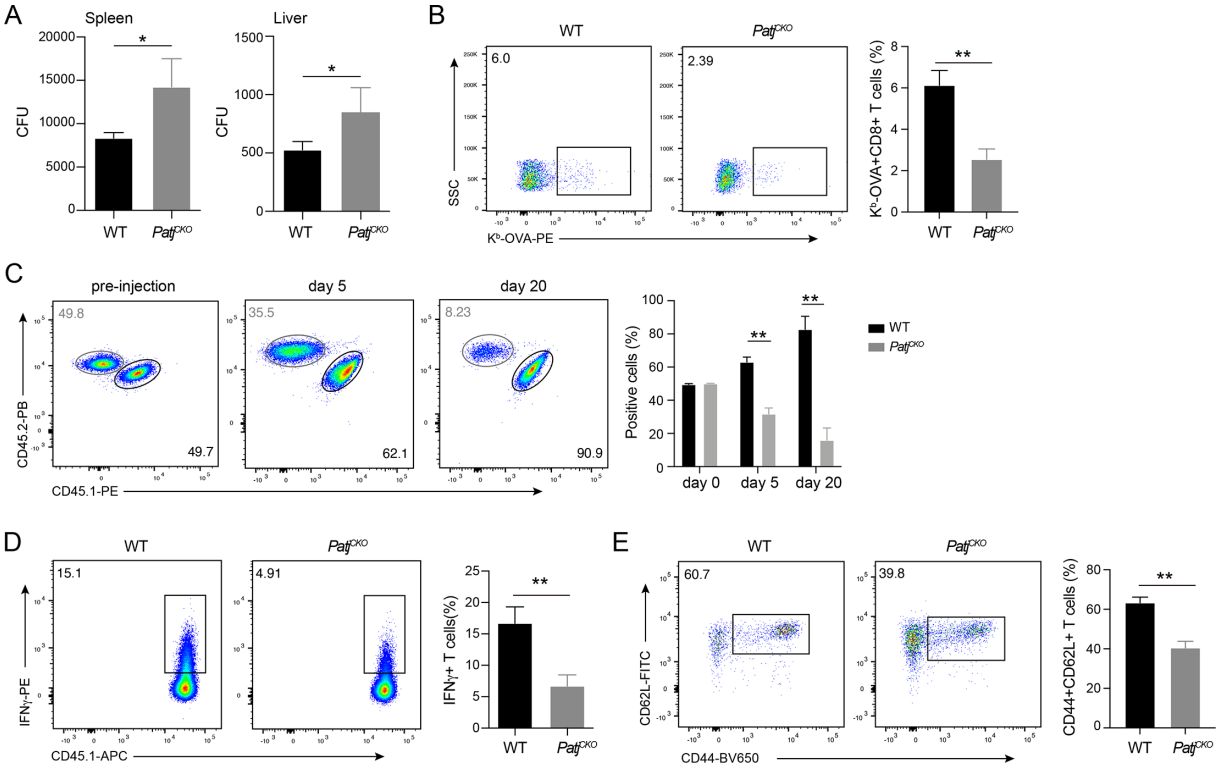

Figure 2 PATJ deficiency impedes T cell-mediated immunity against infections. (A) The bacterial burden in the spleen and liver was quantified of *Patj*^{CKO} and WT mice on day 5 challenged with LM-OVA (n=6). (B) The expression of OVA/H-2 Kb in *Patj*^{CKO} and WT OT-I mice challenged with LM-OVA. (C) A 1:1 mixture of *Patj*^{CKO} (CD45.2+) and WT (CD45.1+CD45.2+) OT-I CD8+T cells was intravenously transferred into mice (CD45.1+) infected with LM-OVA and the frequencies of *Patj*^{CKO} and WT OT-I T cells were assessed by flow cytometry. (D) Production of IFNγ was determined by flow cytometry in *Patj*^{CKO} and WT OT-I T cells. (E) The frequency of memory T cells in *Patj*^{CKO} and WT OT-I mice infected with LM-OVA on day 45. Data are presented as mean±SD. Statistical significance was determined using two-way ANOVA and unpaired t-tests. **p<0.01. ANOVA, analysis of variance; CFU, colony forming unit; IFNγ, interferon-gamma; LM-OVA, *Listeria monocytogenes* expressing ovalbumin; PATJ, PALS1-associated tight junction protein; WT, wild type.

effector functions when activated with anti-CD3 and anti-CD28 antibodies. *Patj*-deficient T cells exhibited reduced cell proliferation (figure 1E) and decreased production of interferon-gamma (IFNγ) and TNFα (figure 1F,G) compared with WT T cells. Taken together, these findings demonstrated that PATJ influences T cell differentiation and may enhance CD8+ T cell degranulation and cytotoxicity.

PATJ deficiency impedes T cell-mediated immunity against infections

To elucidate whether PATJ influences the CD8+ T cell immune response against pathogens, we employed *L. monocytogenes* infection as an acute infection model. Both *Patj*^{CKO} and WT mice were challenged with LM-OVA. The bacterial burden in the spleen and liver was quantified on day 5 postinfection. Compared with WT mice, a significant increase in the level of LM-OVA was observed in the liver and spleen of *Patj*^{CKO} mice (figure 2A). To assess the T cell response to bacterial antigens, the frequency of OVA-specific CD8+ T cells in the spleen was assessed by the OVA/H-2 Kb staining. In comparison to control mice, a notable decrease in both the percentage and absolute number of OVA tetramer+CD8+ T cells in the spleen of *Patj*^{CKO} mice on day 7 after infection was observed (figure 2B). This suggested that the absence of *Patj* compromises the T cell response to bacterial infection.

We subsequently mixed WT OT-I T cells (CD45.1+CD45.2+) with *Patj*^{CKO} OT-I T cells (CD45.2+) at a 1:1 ratio and transferred them into C57BL/6 recipient mice (CD45.1+). On the following day, the recipient mice were infected with LM-OVA. The frequencies of effector and memory OT-I T cells in the blood were examined on days 5 and 45 postinfection, respectively. The ratio of these two groups of T cells indicated less proliferation of *Patj*^{CKO} OT-I T cells compared to WT control (figure 2C and online supplemental figure S1). We also discovered that *Patj*^{CKO} OT-I T cells produced significantly fewer effector T cells (figure 2D) and memory T cells (figure 2E) than their WT counterparts. These findings provide evidence that the expression of PATJ in T cells is essential for the immune response against bacterial infection.

Deficiency in PATJ impairs CD8+ T cell response and compromises antitumor activity

Based on the findings above, we aim to investigate whether the lack of *Patj* directly impairs antitumor immunity. We found that the absence of *Patj* did not impact the

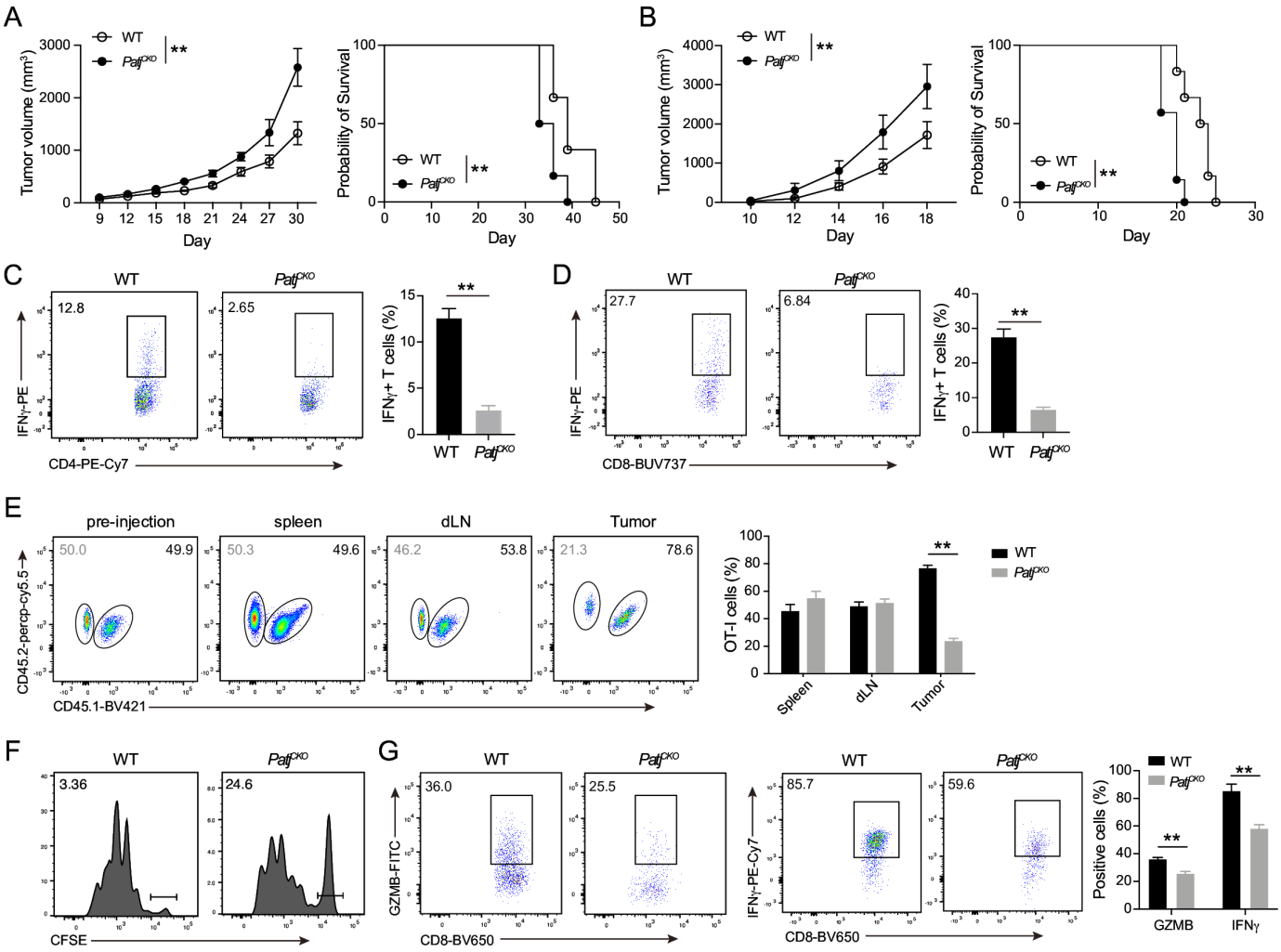

Figure 3 Deficiency in PATJ impairs CD8+ T cell response and compromises antitumor activity. (A) Tumor progression and overall survival rates in wild-type or *Patj*^{CKO} mice following subcutaneous implantation of MC38 cells. (B) Comparative analysis of tumor growth and survival outcomes in WT and *Patj*^{CKO} mice after subcutaneous inoculation with B16 cells. Tumor volume was measured every other day (mean±SEM, **p<0.01) (Left). The survival curves of the three groups were compared (right). Statistical significance was assessed by the two-way ANOVA (left), or log-rank (Mantel-Cox) test of survival curve (right). (C-D) IFNγ production was measured in CD4+ and CD8+ T cells from B16 tumors and stimulated with phorbol myristate acetate (PMA) and ionomycin in vitro using flow cytometry. (**E**) A 1:1 mixture of *Patj*^{CKO} (CD45.2+) and WT (CD45.1+CD45.2+) OT-I CD8+ T cells was intravenously transferred into mice (CD45.1+) bearing B16-OVA tumors. The frequency of *Patj*^{CKO} and WT OT-I T cells was assessed by flow cytometry in the spleen, draining lymph nodes, and TILs. (**F**) Proliferation rates of *Patj*^{CKO} and WT OT-I CD8+ T cells within B16-OVA tumors were evaluated. (**G**) Production of IFNγ and GZMB was determined by flow cytometry in *Patj*^{CKO} and WT OT-I T cells isolated from tumors and stimulated with PMA and ionomycin *in vitro*. Data are presented as mean±SD. Statistical significance was determined using Two-way ANOVA and unpaired t-tests. **p<0.01. ANOVA, analysis of variance; CFSE, carboxyfluorescein succinimidyl ester; dLN, draining lymph nodes; IFNγ, interferon-gamma; FITC, fluorescein isothiocyanate; PATJ, PALS1-associated tight junction protein; TILs, tumor infiltrating lymphocytes; WT, wild type.

development of thymocytes (online supplemental figure S2). However, the mice without *Patj* exhibited increased tumor growth and reduced survival rates when challenged with MC38 (figure 3A) or B16 (figure 3B) tumor cells, highlighting the significance of Patj in promoting antitumor immunity. Further analyses of the tumor-infiltrating T cells revealed that *Patj*^{CKO} CD4+ and CD8+ T cells had reduced function, as evidenced by decreased production of cytokines such as IFNγ (figure 3C,D).

Subsequently, we evaluated whether PATJ modulates T cell-intrinsic antitumor immunity. To this end, we mixed *Patj*^{CKO} OT-I cells (CD45.2+) and WT OT-I cells (CD45.1+CD45.2+), labeled with CFSE, at a ratio of 1:1, and then transferred them into B16-OVA tumor-bearing mice via tail vein injection. A significant decrease in *Patj*^{CKO} OT-I T cell number was observed within B16-OVA tumors (figure 3E and online supplemental figure S1). Intratumoral CD8+ OT-I T cells from *Patj*^{CKO} mice exhibited reduced proliferation compared with controls (figure 3F). Furthermore, intratumoral CD8+ OT-I T cells in *Patj*^{CKO} mice exhibited decreased expression of IFNγ and granzyme B (figure 3G). Thus, our data indicated that PATJ is critical in the accumulation and effector function of CD8+T cells in tumors.

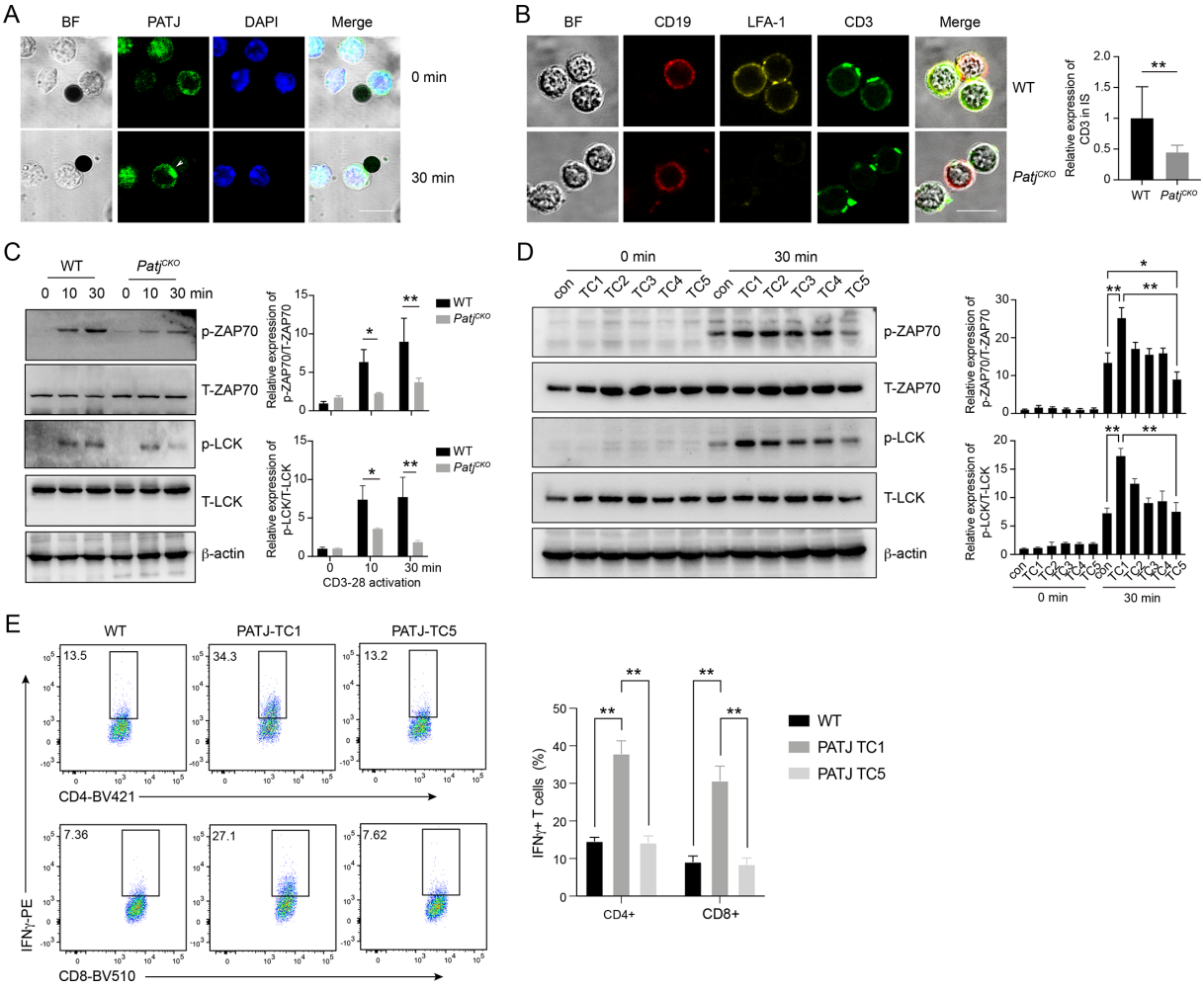

Figure 4 PATJ polarizes to the T cell synapse in response to TCR triggering. (A) The expression of Patj in CD8+ T co-cultured with CD3/CD28 activation beads by IF staining. BF, bright field; Bar=20 µm. (B) The synapse formation of B cells pulsed with $OVA_{257–264}$ (SIINFEKL) peptides and OT-I T cells from *Patj*^{CKO} and WT mice was analyzed by confocal imaging. The expression of CD3 in the IS was analyzed using Image J software (right). (C) The expression of TCR signaling in CD8+ T from *Patj*^{CKO} and WT mice activated with anti-CD3/28 antibodies. (D) The expression of TCR signaling in CD8+ T from WT mice transduced with PATJ truncate activated with anti-CD3/28 antibodies. (E) Production of IFNγ was determined by flow cytometry in CD8+ T from WT mice transduced with PATJ truncate activated with anti-CD3/28 antibodies. Data are presented as mean±SD. Statistical significance was determined using unpaired t-tests and two-way ANOVA. *p<0.05, and **p<0.01. ANOVA, analysis of variance; DAPI, 4',6-diamidino-2-phenylindole IF, immunofluorescence; IFNγ, interferon-gamma; PATJ, PALS1-associated tight junction protein; TCR, T cell receptor; WT, wild type.

PATJ polarizes to the T cell synapse in response to TCR triggering

To determine whether PATJ is involved in T cell receptor (TCR) triggering, we examined the localization of Patj in CD8+T cells during activation by anti-CD3/CD28 beads. We found that Patj polarized towards the interface of T cells with anti-CD3/CD28 beads, potentially contributing to the formation of the immune synapse (figure 4A). We further explored Patj localization during immune synapse formation of OT-I T cells incubated with B cells pulsed with $OVA_{257–264}$ (SIINFEKL) peptides, serving as antigen-presenting cells (APCs). The formation of the immune synapse was confirmed by the recruitment of CD3 to the interface between T cells and B cells, as well as the polarization of LFA-1. Reduced recruitment of CD3 and LFA-1 to the immune synapse was observed in *Patj*^{CKO} OT-I incubated with $OVA_{257–264}$ peptide-pulsed B cells (figure 4B). We also examined the expression of Patj during the formation of the IS. As anticipated, Patj was notably enriched at the IS (online supplemental figure S3A).

Interestingly, *Patj*^{CKO} T cells express low levels of LFA-1 (online supplemental figure S3B). To check if PATJ affects IS formation by downregulating LFA-1, we reconstituted LFA-1 in *Patj*^{CKO} OT-I T cells by transducing a retrovirus encoding the LFA-1 cDNA. Subsequent IS analysis showed that *Patj*^{CKO} T cells with LFA-1 overexpression still exhibited impaired IS, indicating that the role of Patj in T cell activation is independent of LFA-1 (online supplemental figure S3C,D). We further tested if Patj regulates the expression of other synapse-forming molecules. TCR expression evaluated by FACS staining

of TCRVβ chain showed no difference between the WT and *Patj*^{CKO} T cells (online supplemental figure S3E). Similar expression of CD2, CD28, ICOS, and CD45 was also observed using qPCR (online supplemental figure S3F). Collectively, these findings demonstrated that the impaired TCR signaling activation in *Patj*^{CKO} T cells is not a result of impaired expression of proteins involved in the IS structure, supporting the critical role of PATJ in mediating protein interaction by PDZ domain during T cell activation and synapse formation.

Since IS formation is important for TCR clustering, primary WT and *Patj*^{CKO} CD8+ T cells were stimulated *in vitro* with anti-CD3/CD28. Proximal TCR signaling events, crucial for T-cell activation and proliferation, were evaluated by western blot assay. In T cells lacking *Patj*, we observed markedly diminished phosphorylation of ZAP-70 and LCK compared with the control (figure 4C), indicating Patj's involvement in TCR signaling activation. Consequently, the more efficient establishment of a mature IS and the activation of TCR signaling could explain the enhanced killing capability of Patj CD8+ T cells.

To gain further insight into the PATJ domain in regulating the TCR signals, we next examined the impact of the different PDZ structural domains of Patj on TCR signaling activation. Notably, *in vitro* stimulation of CD8+ T cells overexpressing Patj PDZ domain 1 and 2 with CD3/28 antibodies substantially enhanced TCR signaling compared with WT and other PDZ domains (figure 4D). Consistent with the T cell activation, the expression of IFNγ was also elevated in CD8+ T cells overexpressing Patj PDZ1 and PDZ2 (figure 4E). All together, these results demonstrate that PATJ participates in TCR signal transduction by enhancing IS formation.

PDZ domain in PATJ enhances CAR-T cell activity

MSLN has recently gained significant attention as a crucial target for developing innovative immunotherapeutic strategies.[14] Over the past decade, initial clinical trials have been conducted to assess the efficacy of anti-MSLN CAR T cells against various MSLN-expressing solid tumor malignancies.[15] To further explore the cytolytic potential of these engineered T cells, we co-cultured MSLN CAR T cells with A549 cells that overexpress MSLN. Notably, the MSLN CAR.PATJ TC1 (MSLN-TC1 CAR) T cells displayed enhanced killing activity against A549 tumor cells compared with conventional MSLN CAR T cells across all evaluated E:T ratios (figure 5A). To evaluate the sequential killing activity of CAR-T cells, we employed a repeated *in vitro* challenge assay. MSLN CAR-T cells were incubated with A549$^{\text{MSLN-GFP-luciferase}}$ cells at an E:T ratio of 2:1. Every 48 hours, the CAR-T cells were removed,

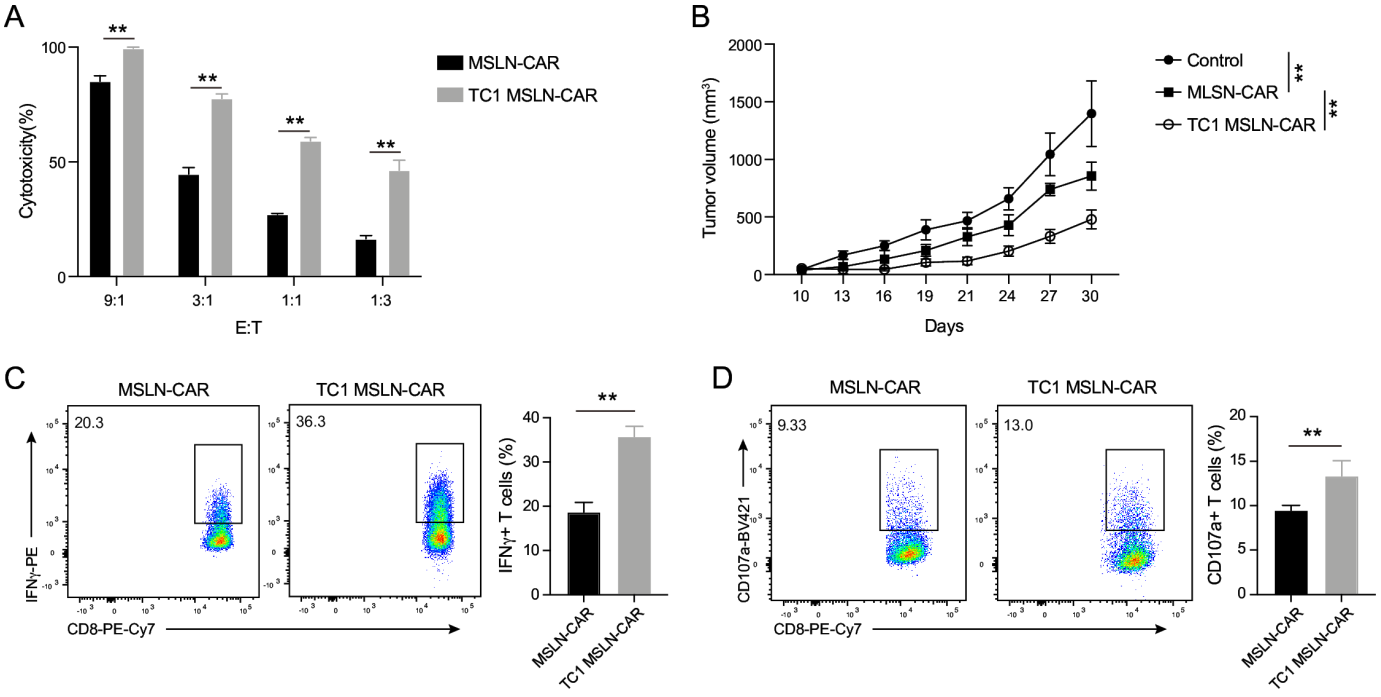

Figure 5 PDZ domain in PATJ enhances CAR-T cells activity. (A) Cytotoxicity assay was assessed using the LDH assay after a 24-hour co-culture of A549$^{\text{MSLN}}$ lung adenocarcinoma cells with MSLN CAR T and MSLN-TC1 CAR cells. (B) Tumor growth kinetics of A549$^{\text{MSLN}}$ cells implanted subcutaneously in NSG mice treated with MSLN CAR T or MSLN-TC1 CAR cells, with treatment initiation on day 12 post-tumor inoculation. (C) IFNγ production was measured by flow cytometry in NSG tumor-bearing mice treated with MSLN CAR T or MSLN-TC1 CAR T cells. (D) The expression of CD107a was measured by flow cytometry of A549$^{\text{MSLN}}$ lung adenocarcinoma cells with MSLN CAR T and MSLN-TC1 CAR (E:T=1:3) cells *in vitro*. Data are presented as mean±SD or mean±SEM (tumor volume). Statistical significance was determined using two-way ANOVA or unpaired t-tests. **p<0.01. ANOVA, analysis of variance; CAR, chimeric antigen receptor; E:T, effector-to-target; IFNγ, interferon-gamma; LDH, lactate dehydrogenase; MSLN, mesothelin; PATJ, PALS1-associated tight junction protein.

counted, and reincubated with A549$^{MSLN\text{-}GFP\text{-}luciferase}$ target cells at the same 2:1 E:T ratio to evaluate sequential killing activity. Our results demonstrated that CAR-T cells overexpressing PATJ TC1 exhibited significantly enhanced capacity for continuous target cell elimination compared with the control group (online supplemental figure S4A). Subsequently, we compared the immune synapses of PATJ TC1 to WT MSLN CAR-T cells formed with A549$^{MSLN\text{-}EGFP}$ target cells. We found an increased clustering of LFA-1 and CD3 at the IS in the PATJ TC1 group compared with the control group (online supplemental figure S4B). This finding indicates that PATJ TC1 overexpression promotes the formation of the IS in CAR-T cells, thereby activating the TCR signaling pathway and enhancing the cytotoxicity of CAR-T cells against tumor cells.

Next, we assessed the antitumor effectiveness of unmodified T cells, MSLN CAR T cells, and MSLN-TC1 CAR T cells in solid tumor xenograft models. Using an A549^{MSLN} lung adenocarcinoma model, tumor cells were implanted s.c., followed by intravenous administration of CAR-T cells 14 days later. Tumors treated with unmodified T cells exhibited rapid growth. On the other hand, MSLN CAR and MSLN-TC1 CAR T cells exhibited antitumor activity. However, mice treated with MSLN-TC1 CAR T cells showed a significant improvement in tumor suppression compared with those treated with MSLN CAR T cells (figure 5B). According to flow cytometry analysis, MSLN-TC1 CAR T cells produced a higher amount of IFNγ (figure 5C) and CD107a (figure 5D) compared with their MSLN CAR counterparts. These results strongly suggest that incorporating the PDZ domain of PATJ in CAR-T cells confers potent antitumor activity.

DISCUSSION

The development of adaptive immunity depends on the effective induction of an antigen-specific T cell response.[16] A coordinated interaction between T cells and APCs establishes the IS, which serves as a signaling platform essential for efficient TCR activation.[17] On the TCR is appropriately engaged, signals are transmitted that result in T cell development, activation, and effector function, with scaffolding proteins playing pivotal roles in synapse formation.[18] Furthermore, modifying the synapse by adding a binding site for intracellular scaffolding proteins to the CAR has led to an efficient and effective CAR T therapy for solid tumors.[11] Some proteins containing PDZ domains assist in synapse formation and the polarity of immune cells.[19] Our study discovered that PATJ is recruited to the IS through its PDZ domain, triggering TCR signaling activation, which enhances both antitumor immunity and anti-inflammatory responses, thus providing a novel target for cancer immunotherapy.

PDZ domains were identified through sequence homology in proteins such as PSD-95, Dlg, and ZO-1. These domains, which can range from 2 to over 10 per protein, are typically found in proteins localized to specific subcellular regions near the plasma membrane in polarized cells.[20] Esther González-Mancha *et al* demonstrated that SNX27, a PDZ domain-containing protein, polarizes to the IS on TCR activation.[21] Proteins from the Scribble, Crumbs3, and Par3 complexes, known for their role in epithelial polarity regulation, also exhibit polarization in T cells with ISs.[9 19] The recruitment of hDlg to the synapse modulates T cell function and polarity by selectively binding PDZ motif-containing proteins.[9] Given the importance of cell polarization for T cell migration, proliferation, homotypic interactions, activation following antigen presentation, and cytotoxicity,[22] further investigation into the scaffolds and signals governing T cell polarization is warranted.

The multi-PDZ domain protein PATJ is instrumental in stabilizing the Crumbs-Pals1 complex, which is essential for maintaining epithelial cell polarity and facilitating tight junction formation. This complex is critical for preventing the interchange of cell membrane components, thereby maintaining cellular polarity.[23] Although the function of PATJ in immune cells, especially T cells, is not extensively documented, our observations within the first 6 hours post-activation reveal a transient increase in Patj expression in CD8+ T cells, followed by downregulation after 12 hours and a continued decline in expression in vitro over time. Furthermore, our analysis of RNA sequencing datasets also revealed elevated levels of PATJ transcripts in CD8+ T cells with a terminal effector phenotype compared with those with a memory phenotype. Patj mRNA was observed to be upregulated at 6 hours, whereas the protein level did not significantly increase until 12 hours later. This delay may be attributed to a combination of factors, including a relatively low translation rate of the Patj mRNA and/or the inherent stability of the Patj protein. These findings suggest a correlation between PATJ and the early activation state of CD8+ T cells.

Given its distinctive role in CD8+ T cells, we implemented a conditional knockout of *Patj* in T cells to investigate whether the deficiency of *Patj* could augment antitumor immunity. On activation, the effector function and proliferation of *Patj*^{CKO} CD8+ T cells were notably suppressed compared with their WT counterparts. Considering that the proliferation of *Patj*-deficient T cells is already impaired 24 hours poststimulation, these deficits are likely to exacerbate over time, potentially contributing to the significant reduction of *Patj*^{CKO} T cells at the zenith of the IS. Consequently, *Patj*^{CKO} mice exhibited larger tumor sizes and reduced survival durations, with CD8+ T cells displaying diminished activation phenotypes. Additionally, adoptive T-cell transfer therapy showed inhibited antitumor activity in *Patj*^{CKO} OT-I cytotoxic T lymphocytes.

To elucidate the mechanism underlying the impaired effector functions and proliferation in *Patj*-deficient

CD8+T cells, we focused on the PDZ domain's role in the IS, a structure vital for directing cytolytic granule secretion in CD8+ T cells to eliminate target cells selectively.[24] Our studies revealed that *Patj*-deficient T cells showed an inability to form or maintain stable interactions with cognate APCs during early T cell activation. Given the role of various molecules in stabilizing T cell-APC interactions and their impact on LFA-1 organization and localization,[25] we assessed LFA-1 accumulation at the IS in $Patj^{CKO}$ T cells. We observed a significant reduction in LFA-1 localization there. Furthermore, examining the potential for suppressed TCR signaling—a key pathway in T cell activation and proliferation—we found that downstream TCR stimulation protein expression was markedly downregulated in activated $Patj^{CKO}$ CD8+ T cells compared with WT cells, suggesting impaired synapse formation and subsequent signaling inhibition.

Signaling molecules at the IS enhance efficiency and shield against inhibitory phosphatases. In contrast, CAR:antigen complexes form atypical synapses that differ from the standard TCR synapse structure.[26] PDZ binding motifs promote synapse formation and polarization in NK CAR cells, enhancing cytotoxicity against tumor cells and survival in solid tumor environments.[11] To dissect the role of the PDZ domain in PATJ, we transfected T cells with truncated Patj PDZ domain vectors. Cells expressing a Patj variant with the first two PDZ domains showed increased phosphorylation of ZAP70 and LCK, and elevated IFNγ production. Moreover, MSLN-TC1 CAR T cells with this Patj truncation exhibited superior antitumor activity and IFNγ levels, correlating with improved survival compared with those treated with standard MSLN-CAR T cells.

Our study provides novel insights into the role of PATJ in T cell activation and IS formation. We found that PATJ is not essential for TCR signaling or T cell activation but is critical for initial T cell-APC interactions. Modifying the synapse using PATJ's PDZ domain emerged as a potential strategy to enhance CAR-T therapies. PATJ's role in synapse formation indicates it as a candidate for therapeutic intervention. Future studies should identify PATJ interactors within the TCR network to clarify its impact on T cell fate and function.

Contributors All authors contributed to the conception and design of the study. PZ, WL, and XX conceptualized the study and designed the experiments. XX and PZ analyzed data, and wrote the manuscript. DW provided the patient samples, and analyzed the data. LX participated in the revision of the manuscript. SC, JH, and XZ provided technical advice. ZF and JZ provided mouse models. PZ is responsible for the overall content as guarantor. All authors have read and approved the final version of the manuscript.

Funding This study is supported by grants from the National Nature Science Foundation in China (NSFC) (82273179, 82192892, 82130086), the Science and Technology Program of Guangzhou (202201010916), National key research and development plan project 22 (2023YFE0205900), and Major science and technology innovation 2030 project (2023ZD0502505).

Competing interests No, there are no competing interests.

Patient consent for publication Not applicable.

Ethics approval Not applicable.

Provenance and peer review Not commissioned; externally peer reviewed.

Data availability statement Data are available upon reasonable request. The datasets used and/or analyzed during the current study are available from the corresponding authors on reasonable request.

ORCID iD

Xinxin Xiong http://orcid.org/0000-0001-9329-6370

REFERENCES

1 Prokhnevska N, Cardenas MA, Valanparambil RM, *et al*. CD8$^+$ T cell activation in cancer comprises an initial activation phase in lymph nodes followed by effector differentiation within the tumor. *Immunity* 2023;56:107–24.
2 Kearney CJ, Brennan AJ, Darcy PK, *et al*. The Role of the immunological Synapse Formed by Cytotoxic Lymphocytes in Immunodeficiency and Anti-Tumor immunity. *Crit Rev Immunol* 2015;35:325–47.
3 Gardiner J, Overall R, Marc J. PDZ domain proteins: 'dark matter' of the plant proteome? *Mol Plant* 2011;4:933–7.
4 Liu X, Fuentes EJ. Emerging Themes in PDZ Domain Signaling: Structure, Function, and Inhibition. *Int Rev Cell Mol Biol* 2019;343:129–218.
5 Nourry C, Grant SGN, Borg J-P. PDZ domain proteins: plug and play! *Sci STKE* 2003;2003.
6 Kim E, Sheng M. PDZ domain proteins of synapses. *Nat Rev Neurosci* 2004;5:771–81.
7 Xavier R, Rabizadeh S, Ishiguro K, *et al*. Discs large (Dlg1) complexes in lymphocyte activation. *J Cell Biol* 2004;166:173–8.
8 Krummel MF, Macara I. Maintenance and modulation of T cell polarity. *Nat Immunol* 2006;7:1143–9.
9 Ludford-Menting MJ, Oliaro J, Sacirbegovic F, *et al*. A network of PDZ-containing proteins regulates T cell polarity and morphology during migration and immunological synapse formation. *Immunity* 2005;22:737–48.
10 Yeh JH, Sidhu SS, Chan AC. Regulation of a late phase of T cell polarity and effector functions by Crtam. *Cell* 2008;132:846–59.
11 Chockley PJ, Ibanez-Vega J, Krenciute G, *et al*. Synapse-tuned CARs enhance immune cell anti-tumor activity. *Nat Biotechnol* 2023;41:1434–45.
12 Wang WJ, Lyu TJ, Li Z. Research Progress on PATJ and Underlying Mechanisms Associated with Functional Outcomes After Stroke. *Neuropsychiatr Dis Treat* 2021;17:2811–8.
13 Buckley CE, St Johnston D. Apical-basal polarity and the control of epithelial form and function. *Nat Rev Mol Cell Biol* 2022;23:559–77.
14 Faust JR, Hamill D, Kolb EA, *et al*. Mesothelin: An Immunotherapeutic Target beyond Solid Tumors. *Cancers (Basel)* 2022;14:1550.
15 Klampatsa A, Dimou V, Albelda SM. Mesothelin-targeted CAR-T cell therapy for solid tumors. *Expert Opin Biol Ther* 2021;21:473–86.
16 Tippalagama R, Chihab LY, Kearns K, *et al*. Antigen-specificity measurements are the key to understanding T cell responses. *Front Immunol* 2023;14:1127470.
17 Dustin ML. The immunological synapse. *Cancer Immunol Res* 2014;2:1023–33.
18 Shaw AS, Filbert EL. Scaffold proteins and immune-cell signalling. *Nat Rev Immunol* 2009;9:47–56.

19 Barreda D, Gutiérrez-González LH, Martínez-Cordero E, *et al*. The Scribble Complex PDZ Proteins in Immune Cell Polarities. *J Immunol Res* 2020;2020:5649790.
20 Christensen NR, Čalyševa J, Fernandes EFA, *et al*. PDZ Domains as Drug Targets. *Adv Ther (Weinh)* 2019;2:1800143.
21 González-Mancha N, Rodríguez-Rodríguez C, Alcover A, *et al*. Sorting Nexin 27 Enables MTOC and Secretory Machinery Translocation to the Immune Synapse. *Front Immunol* 2021;12:814570.
22 Blanchard N, Di Bartolo V, Hivroz C. In the immune synapse, ZAP-70 controls T cell polarization and recruitment of signaling proteins but not formation of the synaptic pattern. *Immunity* 2002;17:389–99.
23 Fiedler J, Moennig T, Hinrichs JH, *et al*. PATJ inhibits histone deacetylase 7 to control tight junction formation and cell polarity. *Cell Mol Life Sci* 2023;80:333.
24 Dustin ML, Chakraborty AK, Shaw AS. Understanding the structure and function of the immunological synapse. *Cold Spring Harb Perspect Biol* 2010;2:a002311.
25 Springer TA, Dustin ML. Integrin inside-out signaling and the immunological synapse. *Curr Opin Cell Biol* 2012;24:107–15.
26 Xiong Y, Libby KA, Su X. The physical landscape of CAR-T synapse. *Biophys J* 2024;123:2199–210.